Translational Oncology
www.transonc.com

Volume 11 Number 6 December 2018 pp. 1370–1378 1370

Determination of Hepatocellular Carcinoma and Characterization of Hepatic Focal Lesions with Adaptive Multi-Exponential Intravoxel Incoherent Motion Model

Hong-Xia Zhang[*,1], Xiu-Shi Zhang[*,1], Zi-Xiang Kuai[*], Yang Zhou[*], Yun-Feng Sun[*], Zhi-Chang Ba[*], Kuang-Bang He[*], Xi-Qiao Sang[†], Yuan-Fei Yao[*], Chun-Yu Chu[‡] and Yue-Min Zhu[§]

[*]Imaging Center, Harbin Medical University Cancer Hospital, Harbin, 150081, China; [†]Division of Respiratory Disease, The Fourth Hospital of Harbin Medical University, Harbin, 150001, China; [‡]College of engineering, Bohai University, Jinzhou, 121013, China; [§]CREATIS, CNRS UMR 5220-INSERM U1206-University Lyon 1-INSA Lyon-University Jean Monnet Saint-Etienne, Lyon, 69621, France

Abstract

PURPOSE: To distinguish hepatocellular carcinoma (HCC) from other types of hepatic lesions with the adaptive multi-exponential IVIM model. *METHODS:* 94 hepatic focal lesions, including 38 HCC, 16 metastasis, 12 focal nodular hyperplasia, 13 cholangiocarcinoma, and 15 hemangioma, were examined in this study. Diffusion-weighted images were acquired with 13 b values (b = 0, 3, …, 500 s/mm^2) to measure the adaptive multi-exponential IVIM parameters, namely, pure diffusion coefficient (D), diffusion fraction (f_d), pseudo-diffusion coefficient (D_i*) and perfusion-related diffusion fraction (f_i) of the *ith* perfusion component. Comparison of the parameters of and their diagnostic performance was determined using Mann-Whitney *U* test, independent-sample *t* test, one-way analysis of variance, Z test and receiver-operating characteristic analysis. *RESULTS:* D, D_1* and D_2* presented significantly difference between HCCs and other hepatic lesions, whereas f_d, f_1 and f_2 did not show statistical differences. In the differential diagnosis of HCCs from other hepatic lesions, D_2* (AUC, 0.927) provided best diagnostic performance among all parameters. Additionally, the number of exponential terms in the model was also an important indicator for distinguishing HCCs from other hepatic lesions. In the benign and malignant analysis, D gave the greatest AUC values, 0.895 or 0.853, for differentiation between malignant and benign lesions with three or two exponential terms. Most parameters were not significantly different between hypovascular and hypervascular lesions. For multiple comparisons, significant differences of D, D_1* or D_2* were found between certain lesion types. *CONCLUSION:* The adaptive multi-exponential IVIM model was useful and reliable to distinguish HCC from other hepatic lesions.

Translational Oncology (2018) 11, 1370–1378

Introduction

The intravoxel incoherent motion (IVIM) model was first proposed by Le Bihan in the late 1980s and derives from diffusion-weighted (DW) imaging a combined measurement of the pure molecular motion of water (diffusion) and microcirculation of blood in the complex capillary network (perfusion), thus providing a theoretical framework to calculate diffusion- and perfusion-related parameters with multi-b-value DW images [1,2]. In terms of tumor tissue, this separate diffusion and perfusion estimation is helpful due to the increased cellular density and the increased neovascularity in many

Address all correspondence to: Zi-Xiang Kuai, PhD, Imaging Center, Harbin Medical University Cancer Hospital, Haping Road No.150, Nangang District, Harbin, 150081, China.
E-mail: zixiangkuai@126.com

[1] These authors contributed equally to this work and should be considered co-first authors.

Received 4 August 2018; Revised 27 August 2018; Accepted 27 August 2018

1936-5233/18
https://doi.org/10.1016/j.tranon.2018.08.011

malignant tumors [3]. Additionally, because of growing concerns over side effects of gadolinium-based contrast agent sensitive to tumors, such as renal function impairment and gadolinium deposition in the brain [4,5], the IVIM imaging that do not depend on contrast agent are increasingly used in clinical practice for tumor detection and characterization, especially for the hepatic tumor. The classical bi-exponential IVIM model was consist of two exponential terms and incorporates the pure diffusion coefficient (D), the pseudo-diffusion coefficient (D^*), and the perfusion-related diffusion fraction (f), respectively [2]. Previous studies revealed that the D values can provided relatively high diagnostic performance in differentiating malignant from benign liver lesions [6,7]. But it was also found that there was great overlap of D between benign and malignant liver lesions [8]. Also, no significant differences in the perfusion-related parameters (i.e. f and D^*) were observed between the hepatic tumor types [9]. In other words, the effectiveness of the classical bi-exponential IVIM model to diagnose and differentiate hepatic tumors was rather limited.

Meanwhile, a multi-component perfusion phenomenon was found in the liver and it was explained by the presence of various vessels and flow regimes in the hepatic parenchyma [10–12]. At the same time, an adaptive multi-exponential IVIM model was established to characterize the multiple perfusion components in the liver, where one perfusion component is corresponding to one exponential term [13]. Since more than one exponential term is used to describe hepatic perfusion, the adaptive multi-exponential IVIM model can give more perfusion-related parameters than the classical bi-exponential IVIM model. This is to say that more perfusion-related information can be obtained by using the adaptive multi-exponential IVIM model in contrast to the classical bi-exponential IVIM model with respect to the liver. In fact, the additional perfusion-related information might be potentially helpful for the diagnosis of hepatic focal lesions due to the difference in characteristic vascularity between different types of hepatic lesions. Thus, it could be expected that the adaptive multi-exponential IVIM model has better diagnostic performance than the classical bi-exponential IVIM model for classification/characterization of the hepatic focal lesions.

Previous published studies focused more on the distinction between the benign and malignant liver lesions using the classical bi-exponential IVIM model [14–17]. However, the suggested cutoff values for malignant tumors were quite variable, which would make an accurate diagnosis difficult, even leading to misdiagnosis, conservative treatment, or over-intervention. This considerable variability in the IVIM measurements was mainly attributed to the variable grouping for benign and malignant liver lesions in these studies. In other words, the effort of differentiating malignancies from benign hepatic lesions was heavily discounted owing to the lack of consensus on the grouping of benign and malignant lesions. It was known that hepatocellular carcinoma (HCC) is the most common malignant primary hepatic tumor and is a leading cause of death [18]. Not only that, the treatment of HCC and other some hepatic tumors, such as hemangioma and focal nodular hyperplasia (FNH), is generally different: HCC frequently are candidate for surgical resection or other interventional treatments, whereas hemangioma and FNH is almost always managed conservatively [19,20]. Thus, it is essential for distinction between HCC and other hepatic lesions. At the same time, this distinction is effective since it does not involve the above grouping problem.

Given this background, the purpose of present study was to attempt to differentiate between HCC and other types of hepatic lesions using the adaptive multi-exponential IVIM model.

Materials and Methods

Patients

The study was conducted under the approval of the local institutional review board and informed consent was waived. Between June 2017 and June 2018, 116 patients with clinical suspected hepatic focal lesion or for HCC surveillance, or with indeterminate character of hepatic focal lesion underwent 3.0T MRI in our department. During this period, multi-b-value DWI was included in our routine liver MRI protocol. Twenty-four patients were excluded because of unsatisfactory lesion size and position (lesion diameter less than 2 cm, which can cause large errors in measurement, n = 7; lesions not located in the central-lower part of the right liver lobe where data show higher reproducibility, n = 9), prior radiotherapy and/or chemotherapy treatment (n = 3), unacceptable image quality that interfered with the delineation of lesions or calculation of the IVIM parameters (n = 2), motion of the patient during acquisition (n = 1), and absence of diagnostic proof (n = 2).

The final study population consisted of 92 patients (54 men and 38 women; age range 34–72 years mean age 50.1 years) with a total of 94 tumors. The final diagnosis of hepatic focal lesions was follows: HCC (n = 38), metastasis (n = 16), FNH (n = 12), cholangiocarcinoma (n = 13), and hemangioma (n = 15). One male patient presented two metastases and one female patient presented two hemangiomas. The hypervascular lesions comprised 28 HCCs, 4 metastases (all from endocrine tumor), as well as all hemangioma and FNH, summing to 59 lesions. The hypovascular lesions contained 10 HCCs, 12 metastases (2 from pancreatic adenocarcinoma, 8 from colorectal cancer, and 2 from gastric cancer), and all cholangiocarcinoma, summing to 35 lesions. Lesion diameter ranged from 24 to 132 mm, with a mean (standard deviation) diameter of 57 (30) mm.

Tumor diagnosis was based on pathological proof for 58 lesions (39 results obtained from biopsy [24 HCC, 4 FNH, 3 metastases, and 8 cholangiocarcinomas] and 19 from surgical resections [11 HCC, and 8 metastases]). The final diagnoses of lesions that were not histologically confirmed (n = 36) were established as follows: 1) for HCCs, all lesions showed typical imaging features (i.e. the arterial hyperenhancement and washout on portal or equilibrium phases) according to the AASLD (American Association for the Study of Liver Diseases); 2) for hemangiomas, diagnosis was established by computed tomography (CT) or MRI typical signal characteristics and contrast enhancement pattern, including high and homogeneous signal intensity (SI) on T2-weighted images and strong globular peripheral enhancement followed by centripetal filling seen during the portal and delayed phases on CT/MRI; 3) for FNH, diagnosis was rendered on the basis of typical radiological findings in contrast-enhanced MRI. After injecting liver-specific contrast agent (Primovist, Bayer Vital GmbH, Leverkusen, Germany), the diagnostic patterns were rapid and strong arterial enhancement on arterial phase, washout on portal and equilibrium phase, and isointense/slight hyperintense to the surrounding hepatic parenchyma on hepatobiliary phase; 4) for metastasis, a diagnosis was made when a lesion was found to be irregular or ill-defined borders that presented low T1 SI and variable high T2 SI, peripheral rim enhancement on dynamic acquisition of CT/MRI, and relatively hypoenhancement enhancement on portal or delayed phase in comparison with liver parenchyma, and exhibiting interval growth of at least 20% in the longest axial diameter on serial cross-sectional imaging.

Liver MRI

Magnetic resonance imaging of the liver was performed using a 3.0T clinical whole-body MR imaging system (Ingenia, Philips

Medical Systems, Eindhoven, The Netherlands) and a 32-channel phased-array coil. The patients were positioned headfirst in a supine position and their arms were put over the head in order to reduce artifacts. All examinations were performed on patients fasting for 5 hours. The protocol used consisted of the following sequences: an axial fat-suppressed RT (respiratory-triggered) T2-weighted single-shot turbo spin echo (repetition time (TR)/echo time (TE) 535/75, slice thickness /gap 7/1 mm, field of view (FOV) 350 × 392 cm, matrix size 232 × 199), a coronal breath-hold T2-weighted single-shot turbo spin echo (TR/TE 1100/80, slice thickness /gap 6/1 mm, FOV 350 × 346 cm, matrix size 292 × 253), an axial breath-hold dual-echo (in-phase and opposed-phase) T1-weighted fast field-echo (TR/TE1/TE2 106/1.15/2.3, slice thickness /gap 7/1 mm, FOV 400 × 322 cm, matrix size 244 × 181), a fat-suppressed dynamic 3-dimensional volumetric interpolated breath-hold T1-weighted sequence (TR/TE1/TE2 3.6/1.32/2.3, slice thickness /gap 5/-2.5 mm, FOV 320 × 427 cm, matrix size 200 × 250) before and after bolus injection of gadolinium-based contrast agent. Postcontrast images were collected at the arterial phase (20 seconds), portal venous phase (55 seconds), equilibrium phase (90 seconds), and delayed phase (180 seconds).

IVIM Imaging

The adopted IVIM sequence was based on a RT single-shot spin-echo echo-planar imaging with 13 distinct b values ranging from 0 s/mm^2 to a maximum of 500 s/mm^2 (0, 3, 5, 10, 20, 30, 50, 75, 100, 200, 300, 400, and 500 s/mm^2). Here, the intention of sampling multiple low b values was to accurately calculating perfusion components, whereas relatively small numbers of high b values were sampled was due to the fact measurements at high b values are reported to be stable [21]. The image parameters were as follows: TR/TE 1 respiratory cycle/70 ms, 20 slices, slice thickness/gap 5/0 mm, FOV 400 × 400 mm, matrix size 148 × 148, number of excitations 2. To increase signal-to-noise ratio (SNR), two averages were performed. Motion probing gradients were applied in three orthogonal directions. The total average acquisition time of IVIM imaging was about 6 minutes.

Image Analysis

Regions of interest (ROIs) were placed in consensus within the lesions by two radiologists, one with 15 years and the other 7 years of clinical experience in abdominal MRI, referring to the gadolinium-enhanced MR images. If a lesion manifested homogeneity, a freehand ROI was drawn cautiously along the edge of the lesion while avoiding surrounding vessels or bile ducts structures. If a lesion demonstrated a heterogeneous appearance, ROI were positioned by avoiding necrosis or hemorrhagic areas and artifacts. These ROIs were initially placed on unweighted (i.e. b = 0 s/mm^2) image, then copied and pasted on each corresponding diffusion-weighted image. The exemplary images of a patient with HCC are shown in Figure 1. The mean ROI area was 763.58 mm^2 (range: 340.75–3967.18 mm^2). Because the IVIM imaging assumed isotropic diffusion properties, the images for different b values were normalized by dividing them by the unweighted images, and geometric mean of the images over different motion probing gradients was taken. Additionally, the DW signals in each ROI were averaged to improve the SNR.

The averaged DW signals for each ROI were processed through the adaptive multi-exponential IVIM model. The adaptive multi-exponential IVIM model was proposed by Kuai et al in 2017, which can adaptively adjust the number of exponential terms in the model according to different tissues or lesions [13]. The adaptive adjustment was performed on basis of the application of a specific fitting procedure on a multi-exponential IVIM model.

The multi-exponential IVIM model is expressed as

$$\frac{S(b)}{S_0} = f_d e^{-bD} + \sum_{i=1}^{n} f_i e^{-b\left(D_i^* + D\right)}, \quad (1)$$

where $S(b)$ represents the signal intensity at the given b value, S_0 stands for $S(b)$ for $b = 0$, D is the diffusion coefficient, f_d is the diffusion fraction, f_i and D_i^* designate perfusion-related diffusion fraction and pseudo-diffusion coefficient of the *ith* perfusion component, respectively, and n represents the number of perfusion components or perfusion-related exponential terms.

The number of perfusion-related exponential terms was not previously known in the multi-exponential IVIM model, but was gradually determined by introducing, one-by-one, the DW signal corresponding to lower b-value in fitting process. More details were reported in [13].

Statistical Analysis

For quantitative analysis, the distribution of the calculated adaptive IVIM parameters (i.e. f_d, D, f_i, D_i^*) was given as means ± standard deviations (SDs). The Mann-Whitney U test was used to compare the number of exponential terms (i.e. n+1) in the hepatic focal lesions, namely, the HCC vs other hepatic lesions; benign hepatic lesions vs malignant hepatic lesions; hypervascular hepatic lesions vs hypovascular hepatic lesions. For the adaptive IVIM parameters, the

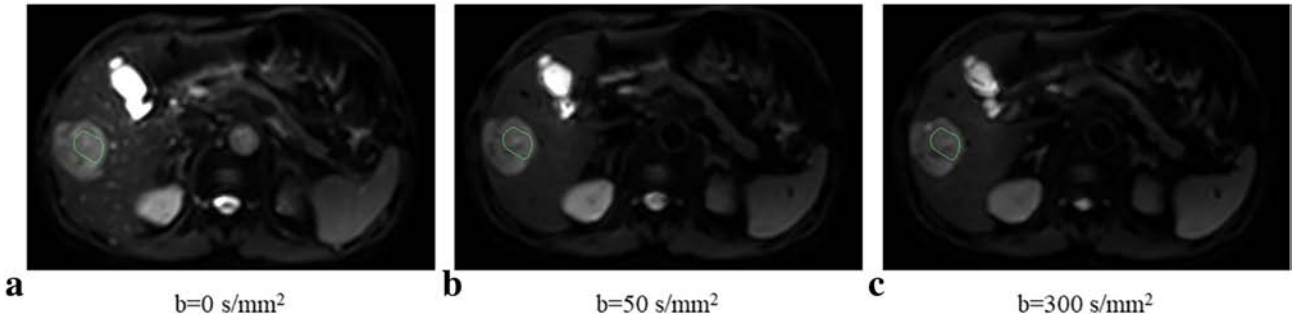

Figure 1. Exemplary axial abdominal MR images with HCC. (a) The image with b = 0 s/mm^2, (b, c) Axial abdominal DW images.

independent-sample *t* test was performed to establish differences between the HCC and other hepatic lesions, between benign hepatic lesions and malignant hepatic lesions, as well as between hypervascular hepatic lesions and hypovascular hepatic lesions, assuming or not the agreement of variance depending on Levene test results. The multiple comparisons among hepatic lesion types (i.e. HCC, metastasis, FNH, cholangiocarcinoma and hemangioma) were performed using one-way analysis of variance (one-way ANOVA) with welch correction. In case of significant differences, detected by one-way ANOVA, Games-Howell and Tukey post hoc tests were applied, respectively, in case of significant or nonsignificant differences among groups variance, revealed by Levene test.

Receiver operating characteristic (ROC) curve analyses were performed and the area under curve (AUC) was obtained to compare the diagnostic performance of each adaptive IVIM parameter for characterization of HCCs from other hepatic lesions and for differentiating benign from malignant hepatic lesions. The sensitivity and specificity of parameters using optimal cutoff values was assessed for a statistical comparison among AUCs using Z test.

All statistical analyses were conducted using commercial software (SPSS, Version 25.0, Chicago, USA; Medcalc, Version 11.4.2.0, Mariakierke, Belgium). Statistical significance was considered for $P < .05$. Additionally, it should be noted that all above comparisons were performed between groups with same number of exponential terms.

Results

HCC vs. Other Hepatic Lesions: Classification

The number of exponential terms and the adaptive IVIM parameters of the HCCs and other hepatic lesions are illustrated in Table 1. It can be observed that the established adaptive multi-exponential IVIM model for each HCC contained three exponential terms, whereas for other hepatic lesions two or three exponential terms were presented in the established models. The Mann-Whitney *U* test showed the significant difference ($P < .001$) in the number of exponential terms between the HCCs and the other hepatic lesions. In terms of the HCC and the hepatic lesions with three exponential terms, the diffusion and pseudo-diffusion coefficients (i.e. D, D_1* and D_2*) were significantly different ($P = .007$, .010, and <.001, respectively) between the two groups, but no significant difference of diffusion and perfusion-related diffusion fractions (f_d, f_1 and f_2) was found in this comparison ($P = .199$, .159 and .310, respectively). The comparison of the HCCs and the hepatic lesions with two exponential terms was not performed since the difference in the number of exponential terms has been apparent between them.

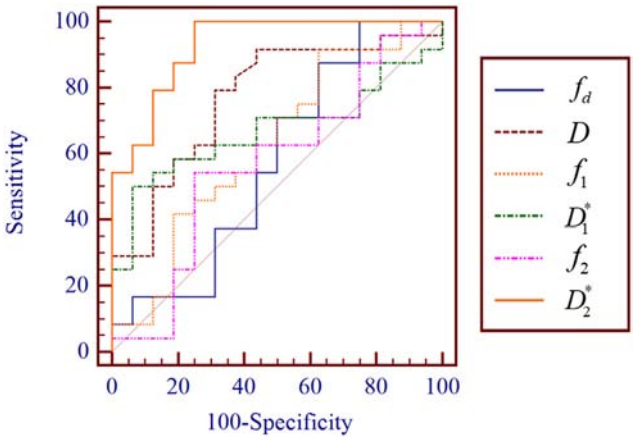

Figure 2. The ROC curves of HCCs vs. other hepatic lesions with three exponential terms for the adaptive IVIM parameters. The line of nondiscrimination is shown by a thin brown line.

The ROC analysis for the HCCs and the hepatic lesions with three exponential terms showed that D_2* (AUC value, 0.927) could be used to distinguish HCCs from other hepatic lesions with most excellent diagnostic ability, at the same time, D (AUC value, 0.770) also presented the superiority over the remaining adaptive IVIM parameters (Figure 2 and Table 2(a)). Using D_2*, an optimal cut-off value of 268.00 × 10^{-3} mm^2/s resulted in a sensitivity/specificity of 98.88%/75.00% for the differentiation between HCCs and other hepatic lesions. Using D, an optimal cut-off value of 1.65 × 10^{-3} mm^2/s resulted in a sensitivity/specificity of 91.67%/56.25% for the differentiation between HCCs and other hepatic lesions. Table 2(b) depicts the differences of AUC values among the adaptive IVIM parameters in Table 2(a). It can be found that the AUC value of parameter D_2* was significantly higher than the parameter f_d, f_1, f_2 and D_1* ($P = .002$, .006, .001, and .007, respectively), but there was no statistically significant difference in the AUC value between D_2* and D ($P = .089 > .05$).

Table 1. The Number of Exponential Terms, Mean ± SD of the Adaptive IVIM Parameters and P Values of the Mann-Whitney *U* Test and the Independent-Sample *t* Test for the Distinction Between the HCCs and the Other Hepatic Lesions

	HCC (38)	Other hepatic lesions (56)		*P*-value
n+1	3 (38)	3 (20)	2 (36)	<.001 *
f_d	0.86±0.05	0.82±0.11	0.87±0.06	.199 †
D (×10^{-3} mm^2/s)	1.20±0.48	1.67±0.52	1.43±0.47	.007 †
f_1	0.09±0.04	0.12±0.08	0.13±0.06	.159 †
D_1 (×10^{-3} mm^2/s)	29.45±20.86	16.56±6.76	72.09±82.21	.010 †
f_2	0.05±0.03	0.06±0.05	–	.310 †
D_2 (×10^{-3} mm^2/s)	424.67±76.87	216.60±108.13	–	<.001 †

HCC = hepatocellular carcinoma.
The number in the parentheses represents the number of hepatic lesions.
* Comparison in the number of exponential terms between the HCCs and the other hepatic lesions using the Mann-Whitney *U* test.
† Comparison in the adaptive IVIM parameter between the HCCs and the other hepatic lesions with three exponential terms using the independent-sample *t* test.

Table 2. (a) Diagnostic Performance of the Adaptive IVIM Parameters for Distinguishing Between the HCCs and the Other Hepatic Lesions with Three Exponential Terms

	AUC	95% CI	Cutoff value (×10^{-3} mm^2/s)	Sensitivity	Specificity
f_d	0.576	0.409 – 0.730	>0.756	98.79%	25.00%
D	0.77	0.609 – 0.888	<=1.649	91.67%	56.25%
f_1	0.625	0.458 – 0.773	<=0.153	91.67%	37.50%
D_1*	0.669	0.503 – 0.810	>20.842	50.00%	93.75%
f_2	0.568	0.402 – 0.723	<=0.035	54.17%	75.00%
D_2*	0.927	0.799 – 0.985	>268.000	98.88%	75.00%

(b) Z Test Results among AUC Comparisons of the Adaptive IVIM Parameters in (a).

	f_d	D	f_1	D_1*	f_2	D_2*
f_d	—	0.083	0.366	0.497	0.937	0.002
D	—	—	0.225	0.401	0.031	0.089
f_1	—	—	—	0.746	0.659	0.006
D_1*	—	—	—	—	0.421	0.007
f_2	—	—	—	—	—	0.001
D_2*	—	—	—	—	—	—

AUC = area under curve.

Table 3. The Number of Exponential Terms, Mean ± SD of the Adaptive IVIM Parameters and *P* Values of the Mann-Whitney *U* Test and the Independent-Sample *t* Test for the Distinction Between the Malignant and the Benign Hepatic Lesions

	Benign Hepatic Lesions (27)		Malignant Hepatic Lesions (67)		*P*-value	
n+1	3 (16)	2 (11)	3 (42)	2 (25)	.004*	
f_d	0.80±0.12	0.85±0.06	0.86±0.05	0.89±0.05	.106†	.180‡
D (×10^{-3} mm^2/s)	1.92±0.41	1.74±0.42	1.19±0.45	1.16±0.31	<.001†	.002‡
f_1	0.13±0.09	0.15±0.06	0.09±0.04	0.11±0.05	.184†	.202‡
D_1* (×10^{-3} mm^2/s)	14.96±3.73	113.80±98.51	27.84±19.74	36.76±28.22	.002†	.042‡
f_2	0.08±0.05	–	0.05±0.03	–	.087†	–
D_2* (×10^{-3} mm^2/s)	214.60±124.94	–	389.55±106.46	–	<.001†	–

The number in the parentheses represents the number of hepatic lesions.

* Comparison in the number of exponential terms between the Malignant and the Benign Hepatic Lesions using the Mann-Whitney *U* test.

† Comparison in the adaptive IVIM parameter between the Malignant and the Benign Hepatic Lesions with three exponential terms using the independent-sample *t* test.

‡ Comparison in the adaptive IVIM parameter between the Malignant and the Benign Hepatic Lesions with two exponential terms using the independent-sample *t* test.

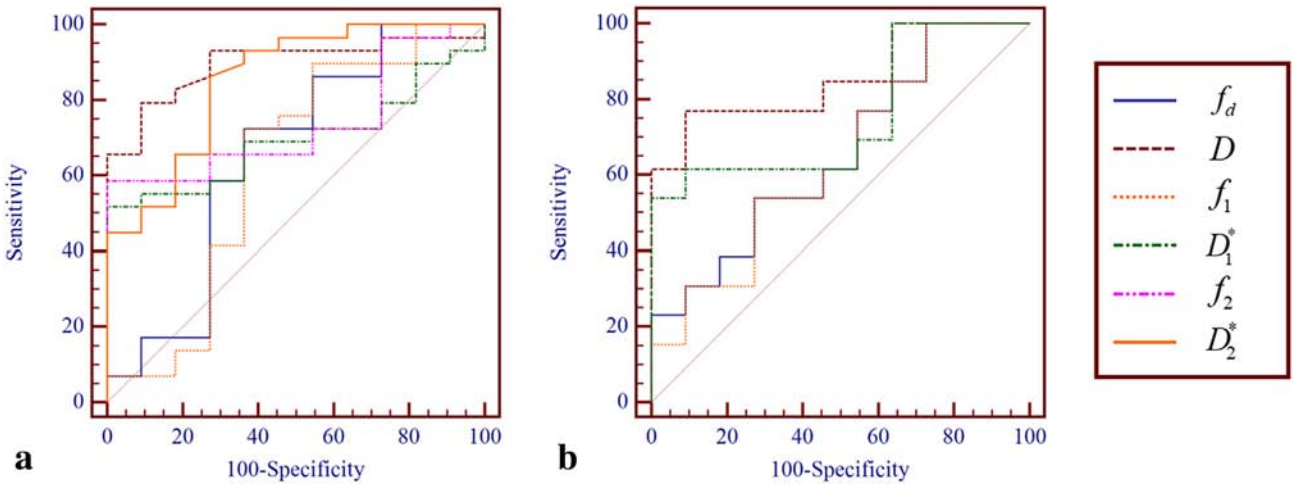

Figure 3. The ROC curves of malignant vs. benign hepatic lesions with three (a) or two (b) exponential terms for the adaptive IVIM parameters. The line of nondiscrimination is shown by a thin brown line.

Benign vs. Malignant Hepatic Lesions: Classification

Table 3 gives the statistical results of the number of exponential terms and the adaptive IVIM parameters from the benign and malignant hepatic lesions. The significant difference (P = .004) in the number of exponential terms can be still found between the benign and malignant groups although the adaptive multi-exponential IVIM models of both benign and malignant groups contained two or three exponential terms. For the comparison between benign and malignant groups with the same number of exponential terms, it can be observed that the D, D_1* and/or D_2* values were significant different (P < .05) between two groups, whereas this significant difference did not appear in the parameters f_d, f_1 and/or f_2 (P > .05).

The ROC curves and corresponding analyses for the adaptive IVIM parameters from benign and malignant groups with three exponential terms are presented in Figure 3*A* and Table 4(a). The ROC-analysis showed the greatest AUC value for D followed by D_2* for the differentiation between malignant and benign lesions with 0.895 and 0.851, respectively. Also, when the cut-off value was set to 1.45 × 10^{-3} mm^2/s and 268 × 10^{-3} mm^2/s for D and D_2* respectively, the best diagnostic performance was obtained correspondingly. But no significant difference (P = .605) was found between D and D_2* in the discriminating malignancy from benign lesions (Table 4(b)). The remaining parameters, f_d, f_1, f_2 and D_1*, were relatively poor malignancy markers, with AUR value less than 0.7, according to the classification system proposed by Swets [22].

In terms of the groups with two exponential terms, D was found to be better than f_d, f_1 and D_1* for discriminating between benign and

Table 4. (a) Diagnostic Performance of the Adaptive IVIM Parameters for Distinguishing Between the Malignant and the Benign Hepatic Lesions with Three Exponential Terms

	AUC	95% CI	Cutoff value (×10^{-3} mm^2/s)	Sensitivity	Specificity
f_d	0.652	0.485–0.795	>0.834	72.41%	63.64%
D	0.895	0.757–0.969	<=1.45	79.31%	90.91%
f_1	0.624	0.457–0.772	<=0.1044	72.41%	63.64%
D_1*	0.696	0.530–0.831	>19.8388	51.72%	98.95%
f_2	0.667	0.574–0.763	<=0.035	58.62%	99.01%
D_2*	0.851	0.703–0.944	>268	86.21%	72.73%

(b) Z Test Results among AUC Comparisons of the Adaptive IVIM Parameters in (a).

	f_d	D	f_1	D_1*	f_2	D_2*
f_d	—	0.054	0.565	0.746	0.456	0.153
D	—	—	0.030	0.055	0.108	0.605
f_1	—	—	—	0.622	0.416	0.107
D_1*	—	—	—	—	0.699	0.191
f_2	—	—	—	—	—	0.320
D_2*	—	—	—	—	—	—

AUC= area under curve.

Table 5. (a) Diagnostic Performance of the Adaptive IVIM Parameters for Distinguishing Between the Malignant and the Benign Hepatic Lesions with Two Exponential Terms

	AUC	95% CI	Cutoff value ($\times 10^{-3}$ mm^2/s)	Sensitivity	Specificity
f_d	0.657	0.438–0.837	>0.785	98.96%	27.27%
D	0.853	0.650–0.963	<=1.361	76.92%	90.91%
f_1	0.623	0.424–0.826	<=0.194	98.97%	27.27%
D_1*	0.755	0.539–0.906	<=16.879	53.85%	99.05%

(b) Z Test Results among AUC Comparisons of the Adaptive IVIM Parameters in (a)

	f_d	D	f_1	D_1*
f_d	—	0.169	0.294	0.532
D	—	—	0.146	0.303
f_1	—	—	—	0.469
D_1*	—	—	—	—

AUC = area under curve.

malignant lesions (Table 5(a) and Figure 3*B*). But no significant difference ($P > .05$) was found between these parameters as malignancy markers (Table 5(b)). Using D, an optimal cut-off value of 1.36×10^{-3} mm^2/s resulted in a sensitivity/specificity of 76.92%/90.91% for discriminating malignancy from benign lesions. Additionally, although the D_1* presented the moderately diagnostical accuracy (0.7<AUC value≤0.9), the its sensitivity was very low (53.85%) when a cut-off value of 16.88×10^{-3} mm^2/s was adopted.

Hypovascular vs. Hypervascular hepatic lesions: Classification

Table 6 summarizes the statistics of the number of exponential terms and the adaptive IVIM parameters from the hypovascular and hypervascular hepatic lesions. The Mann-Whitney U test showed the significant difference ($P = .002$) in the number of exponential terms between two groups. For the groups with three exponential terms, the D_2* was significantly lower in hypovascular than in hypervascular groups ($P = .017$). At the same time, in terms of the groups with two exponential terms, the D and D_1* both were significantly lower ($P < .001$ and $= .016$, respectively) in the hypovascular groups compared with the hypervascular ones. Additionally, no significant difference was observed regarding the other parameters ($P > .05$).

Multiple lesion types: Characterization

The statistical results of the adaptive IVIM parameters by lesion type corresponding to two (represented by "-2") and three (represented by "-3") exponential terms are graphically displayed in Figure 4. The one-way ANOVA followed by Games-Howell or Tukey post hoc tests showed significant differences ($P < .05$) of the diffusion and pseudo-diffusion coefficients (i.e. D, D_1* and/or D_2*) between lesion types. In the comparison between lesions containing three exponential terms, the hemangiomas had significantly higher D value than the HCCs and metastases ($P < .05$); the HCCs presented significantly higher D_1* compared with the hemangiomas and FNHs ($P < .05$), and the difference of the D_1* value between the hemangiomas and FNH can be also observed ($P < .05$); for the parameter D_2*, the significant difference can be found among almost all of lesion types ($P < .05$), with the exception of HCC vs. FNH and metastasis vs. hemangioma. For the lesions containing two exponential terms, the D was significantly higher in hemangiomas than in metastases ($P < .05$), and the D_1* was significantly higher in FNH in comparison with all the other lesions ($P < .05$).

Discussion

The above results suggested that, in contrast to the classical bi-exponential IVIM model, the adaptive multi-exponential IVIM model can indeed provide additional perfusion-related information for certain hepatic focal lesions, especially for the HCCs. In present study, all adaptive multi-exponential IVIM models established on the HCCs incorporated three exponential terms, two of which characterized the HCCs' vascular perfusion. Moreover, the D_2* in the second perfusion-related term (i.e. $f_2e^{-bD_2^*}$) presented the best diagnostic performance (AUC value, 0.927) for the differentiation between HCCs and other hepatic lesions with three exponential terms. The reason for this phenomenon might be duo to the unique form of blood supply in HCC (diameter greater than 2 cm) that the newly formed unpaired hepatic arteries almost completely replace the originally predominant portal veins to supply the tumor. It was known that $D \approx \tau v^2/6$ with τ the time duration after which flowing direction changes and v the blood flowing velocity [23] and the presence of multiple D (e.g. D_1*, D_2*,…, D_n*) is mainly attributed to the difference in the blood flowing velocity (since the velocity is squared) between different types of vessels, such as arteries, veins and capillaries [13]. It was showed that the blood flowing velocity v in the unpaired hepatic arteries or the portal veins is faster than the other vessels in the liver, for example, the hepatic sinusoid capillaries and the hepatic veins [24,25]. Thus, we can infer that the $f_2e^{-bD_2^*}$ was corresponding to the unpaired hepatic arteries or the portal veins, whereas the $f_1e^{-bD_1^*}$ was corresponding to the other hepatic vessels, since the D_2* value was greater than the D_1* value. At the same time, the blood flowing velocity v of the unpaired hepatic arteries were different with the portal veins [24,25]. Therefore, D_2* from HCCs supplied by the unpaired hepatic arteries presented the significant difference compared with other hepatic lesions predominantly perfused by the portal veins.

Table 6. The Number of Exponential Terms, Mean ± SD of the Adaptive IVIM Parameters and *P* Values of the Mann-Whitney *U* Test and the Independent-Sample *t* Test for the Distinction Between the Hypovascular and the Hypervascular Hepatic Lesions

	Hypovascular Lesions (35)		Hypervascular Lesions (59)		*P*-value	
n+1	3 (10)	2 (25)	3 (48)	2 (11)	.002*	
f_d	0.86±0.06	0.89±0.05	0.84±0.08	0.85±0.07	.510†	.091‡
D ($\times 10^{-3}$ mm^2/s)	1.21±0.41	1.17±0.30	1.42±0.56	1.75±0.44	.364†	<.001‡
f_1	0.08±0.05	0.11±0.05	0.10±0.07	0.15±0.06	.441†	.102‡
D_1* ($\times 10^{-3}$ mm^2/s)	14.50±10.20	36.76±27.19	26.38±18.44	113.80±102.90	.116†	.016‡
f_2	0.06±0.03	–	0.05±0.04	–	.884†	–
D_2* ($\times 10^{-3}$ mm^2/s)	261.14±67.09	–	358.32±141.27	–	.017†	–

The number in the parentheses represents the number of hepatic lesions.

* Comparison in the number of exponential terms between the Hypovascular and the Hypervascular Hepatic Lesions using the Mann-Whitney *U* test.

† Comparison in the adaptive IVIM parameter between the Hypovascular and the Hypervascular Hepatic Lesions with three exponential terms using the independent-sample *t* test.

‡ Comparison in the adaptive IVIM parameter between the Hypovascular and the Hypervascular Hepatic Lesions with two exponential terms using the independent-sample *t* test.

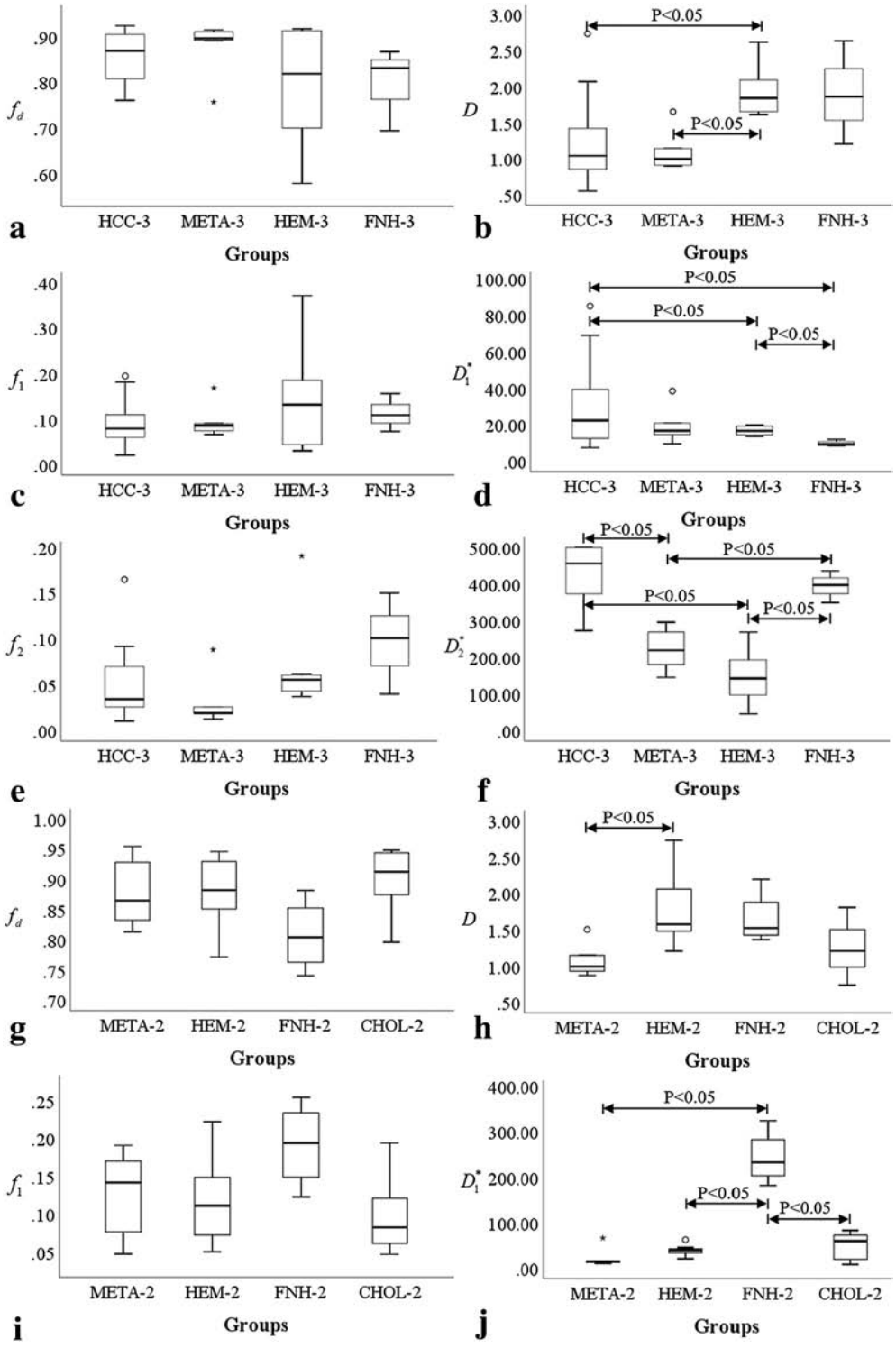

Figure 4. Box plots (median, upper and lower quartiles, maximum and minimum) of the adaptive IVIM parameters for all hepatic lesion types (HCC indicates hepatocellular carcinoma; META, metastasis; HEM, hemangioma; FNH, focal nodular hyperplasia; CHOL, cholangiocarcinoma), whereby (a–f) the comparison among hepatic lesions with three exponential terms (represented by "-3") and (g–j) the comparison among hepatic lesions with two exponential terms (represented by "-2") were presented, respectively.

It can be noted that the significant difference of the D_2* value also appeared in the comparison between the benign and malignant groups or between the hypovascular and hypervascular groups. This might be because the HCCs occupied the majority of the malignant group (38/67) or hypervascular group (38/59), this statistically significant difference of the D_2* value was produced when the malignant or hypervascular group was compared to one's corresponding group consisting of non-HCC lesions. In addition, the significant difference of D_2* can be observed between several independent groups, such as FNH vs. hemangioma and FNH vs. metastasis, which can be to some extent explained by the different pathological changes and discrepancies in perfusion effects between these independent groups [26,27].

The parameter n is another important indicator for distinguishing the HCCs from the other hepatic lesions when the determined adaptive multi-exponential IVIM models on certain non-HCC lesions only contained two exponential terms or one perfusion-related exponential term. The reason why the relatively few perfusion components were detected is, on the one hand, might be owing to the hypovascularity, for example, all hypovascular cholangiocarcinomas and metastases only presented one perfusion component, on the other hand, probably because some occasional pathological responses, such as the scattered thrombi, peripheral inflammatory reaction, vasodilation and increased permeability, reduce or mask the difference between the D_i^* values. Indeed, the too small differences between the D_i^* values were difficultly detected by the adaptive multi-exponential IVIM model unless a very dense b-value distribution was chosen in the acquisition. But more b values mean more longer scanning time, which is unacceptable for the tumor patients.

The accuracy of the parameter D as HCC markers in our study was moderate, with AUC value of 0.77 at best, since the non-HCC lesion group also included the malignant tumors (e.g. the cholangiocarcinomas and metastases) and the parameter D usually gave the close values for the malignant tumors duo to their similar cellularity. That is to say that the D measurement should not be used alone for HCC characterization, but it should be combined with the parameter D_2^*. In present study, the D value was significantly lower in the malignant lesions than in the benign lesions, which accords well with previous reports [3,6,15,17]. As for this reported variability and the differences in specific D values relative to our study, it may be explained by variations in the study populations, acquisition parameters, and lesion size.

Although the parameter D_1^* did not show better performance than the parameters D or D_2^* in the classification of malignancy vs. benignancy or HCC vs. other hepatic lesions, the statistical significance of the D_1^* values can be still observed between them. Also, in aspect of characterizing the hepatic lesion types, the parameter D_1^* also presented the significant difference between certain lesion types. These results suggested that the D_1^* could to some extent assist the parameters D and D_2^* to differentiate hepatic focal lesions. But we should be simultaneously aware of the fact that the significant difference of the D_1^* (or D) value in the bi-exponential IVIM model between the hepatic malignant and benign groups was not be observed in the previous work. In fact, the conclusion that no statistical significance regarding the D value was given by almost all the reports about hepatic lesion characterization. This paradox between the present and previous studies might be attributed to the first introduction of the ultralow b-values, such as 3 and 5 s/mm^2, in present study. Guiu and Cercueil pointed out that the very low b values were needed in order to model the perfusion-related part of the IVIM curve correctly and thus provide reliable results for D, with b values>20 s/mm^2 leading to underestimates of the D value [28].

This study has some limitations. First, no histologic confirmation was available for some hepatic lesions. But the diagnoses for those cases without pathology were made according to their typical imaging features. At the same time, it has been known that different pathological stages of HCC could produce different diffusion and perfusion-related parameters, but which was not pursued because it was beyond the scope of our work. The present study took only the large (or progressed) HCC (i.e. diameter greater than 2 cm) into account. Second, due to the high requirement of the adaptive multi-exponential IVIM model for the SNR of DW signals, ROI-wise instead of voxel-wise analyses were performed in this study. Third, we did not evaluate the inter- and intra-observer agreement or reproducibility of this method. As shown previously, the assessment of reproducibility is essential for each individual measurement using the adaptive multi-exponential IVIM model. Further investigations working on this problem would be expected to facilitate the application of this model in a clinical setting. Finally, although the parameter D_2^* presented the best diagnostic performance for the differentiation between HCCs and other hepatic lesions, the overlap in D_2^* value between two groups still existed. Nevertheless, this problem can be to some extent overcome though combining the parameter D, D_1^* and D_2^* together to achieve this differentiation.

Conclusion

The adaptive multi-exponential IVIM model can indeed give additional perfusion-related parameters compared to the classical bi-exponential IVIM model for certain hepatic focal lesions. Moreover, these additional parameters (e.g. D_2^* and n) that provide superior diagnostic performance could be useful and reliable to distinguish HCC from other types of hepatic focal lesions. Additionally, the adaptive multi-exponential IVIM model was also potentially helpful to differentiate between benign and malignant hepatic focal lesions.

Conflict of Interest

All authors declare that there is no conflict of interest.

Acknowledgements

This work was supported in part by grants from the National Natural Science Foundation of China (No. 81701654, 81703000 and 61601057) and the Fundamental Research Funds for the Provincial Universities (No. 2017LCZX72).

References

[1] Le Bihan D, Breton E, Lallemand D, Grenier P, Cabanis E, and Laval-Jeantet M (1986). MR imaging of intravoxel incoherent motions: application to diffusion and perfusion in neurologic disorders. *Radiology* **161**, 401–407.

[2] Le Bihan D, Breton E, Lallemand D, Aubin ML, Vignaud J, and Laval-Jeantet M (1988). Separation of diffusion and perfusion in intravoxel incoherent motion MR imaging. *Radiology* **168**, 497–505.

[3] Yoon JH, Lee JM, Yu MH, Kiefer B, Han JK, and Choi BI (2014). Evaluation of hepatic focal lesions using diffusion-weighted MR imaging: Comparison of apparent diffusion coefficient and intravoxel incoherent motion-derived parameters. *J Magn Reson Imaging* **39**, 276–285.

[4] Kanda T, Nakai Y, Oba H, Toyoda K, Kitajima K, and Furui S (2016). Gadolinium deposition in the brain. *Magn Reson Imaging* **34**, 1346–1350.

[5] Kartamihardja AA, Nakajima T, Kameo S, Koyama H, and Tsushima Y (2016). Impact of Impaired Renal Function on Gadolinium Retention After Administration of Gadolinium-Based Contrast Agents in a Mouse Model. *Investig Radiol* **51**, 655–660.

[6] Doblas S, Wagner M, Leitao HS, Daire JL, Sinkus R, Vilgrain V, and Van Beers BE (2013). Determination of malignancy and characterization of hepatic tumor type with diffusion-weighted magnetic resonance imaging: comparison of apparent diffusion coefficient and intravoxel incoherent motion-derived measurements. *Investig Radiol* **48**, 722–728.

[7] Ichikawa S, Motosugi U, Ichikawa T, Sano K, Morisaka H, and Araki T (2013). Intravoxel incoherent motion imaging of focal hepatic lesions. *J Magn Reson Imaging* **37**, 1371–1376.

[8] Colagrande S, Regini F, Pasquinelli F, Mazzoni LN, Mungai F, Filippone A, and Grazioli L (2013). Focal liver lesion classification and characterization in noncirrhotic liver: a prospective comparison of diffusion-weighted magnetic resonance-related parameters. *J Comput Assist Tomogr* **37**, 560–567.

[9] Penner AH, Sprinkart AM, Kukuk GM, Gutgemann I, Gieseke J, Schild HH, Willinek WA, and Murtz P (2013). Intravoxel incoherent motion model-based liver lesion characterisation from three b-value diffusion-weighted MRI. *Eur Radiol* **23**, 2773–2783.

[10] Henkelman RM, Neil JJ, and Xiang Q (1994). A quantitative interpretation of IVIM measurements of vascular perfusion in the rat brain. *Magn Reson Med* **32**, 464–469.

[11] Kuai Z-X, Liu W-Y, Zhang Y-L, and Zhu Y-M (2016). Generalization of intravoxel incoherent motion model by introducing the notion of continuous pseudodiffusion variable. *Magn Reson Med* **76**, 1594–1603.

[12] Cercueil J-P, Petit J-M, Nougaret S, Soyer P, Fohlen A, Pierredon-Foulongne M-A, Schembri V, Delhom E, Schmidt S, and Denys A (2014). Intravoxel incoherent motion diffusion-weighted imaging in the liver: comparison of mono-, bi-and tri-exponential modelling at 3.0-T. *Eur Radiol* **25**, 1–10.

[13] Kuai ZX, Liu WY, and Zhu YM (2017). Effect of multiple perfusion components on pseudo-diffusion coefficient in intravoxel incoherent motion imaging. *Phys Med Biol* **62**, 8197–8209.

[14] Luo M, Zhang L, Jiang XH, and Zhang WD (2017). Intravoxel Incoherent Motion Diffusion-weighted Imaging: Evaluation of the Differentiation of Solid Hepatic Lesions. *Transl Oncol* **10**, 831–838.

[15] Watanabe H, Kanematsu M, Goshima S, Kajita K, Kawada H, Noda Y, Tatahashi Y, Kawai N, Kondo H, and Moriyama N (2014). Characterizing focal hepatic lesions by free-breathing intravoxel incoherent motion MRI at 3.0 T. *Acta Radiol* **55**, 1166–1173.

[16] Carodomínguez P, Gupta AA, and Chavhan GB (2017). Can diffusion-weighted imaging distinguish between benign and malignant pediatric liver tumors? *Pediatr Radiol* **48**, 85–93.

[17] Zhu L, Cheng Q, Luo W, Bao L, and Guo G (2014). A comparative study of apparent diffusion coefficient and intravoxel incoherent motion-derived parameters for the characterization of common solid hepatic tumors. **56**, 33–38.

[18] Klauss M, Mayer P, Maier-Hein K, Laun FB, Mehrabi A, Kauczor HU, and Stieltjes B (2016). IVIM-diffusion-MRI for the differentiation of solid benign and malign hypervascular liver lesions—Evaluation with two different MR scanners. *Eur J Radiol* **85**, 1289–1294.

[19] Grazioli L, Morana G, Kirchin MA, and Schneider G (2005). Accurate differentiation of focal nodular hyperplasia from hepatic adenoma at gadobenate dimeglumine-enhanced MR imaging: prospective study. *Radiology* **236**, 166–177.

[20] Donati F, Boraschi P, Gigoni R, Salemi S, Falaschi F, and Bartolozzi C (2013). Focal nodular hyperplasia of the liver: diffusion and perfusion MRI characteristics. *Magn Reson Imaging* **31**, 10–16.

[21] Koh D-M, Collins DJ, and Orton MR (2011). Intravoxel incoherent motion in body diffusion-weighted MRI: reality and challenges. *Am J Roentgenol* **196**, 1351–1361.

[22] Swets JA (1979). Roc Analysis Applied to the Evaluation of Medical Imaging Techniques. *Investig Radiol* **14**, 109–121.

[23] Wetscherek A, Stieltjes B, and Laun FB (2015). Flow-compensated intravoxel incoherent motion diffusion imaging. *Magn Reson Med* **74**, 410–419.

[24] Kudo M (2009). Multistep human hepatocarcinogenesis: correlation of imaging with pathology. *J Gastroenterol* **44**(Suppl. 1), 112–118.

[25] Vollmar B and Menger MD (2009). The hepatic microcirculation: mechanistic contributions and therapeutic targets in liver injury and repair. *Physiol Rev* **89**, 1269–1339.

[26] Ringe KI, Husarik DB, Sirlin CB, and Merkle EM (2010). Gadoxetate disodium-enhanced MRI of the liver: part 1, protocol optimization and lesion appearance in the noncirrhotic liver. *AJR Am J Roentgenol* **195**, 13–28.

[27] Cogley JR and Miller FH (2014). MR imaging of benign focal liver lesions. *Radiol Clin N Am* **52**, 657–682.

[28] Guiu B and Cercueil JP (2011). Liver diffusion-weighted MR imaging: the tower of Babel? *Eur Radiol* **21**, 463–467.